PAPER

Check for updates

Synthesis, structure, and electronic properties of the $Li_{11}RbGd_4Te_6O_{30}$ single crystal†

Zhi-An Zhu,[a] Yu-Cong He,[a] Yang-Yang Lv,[bc] Jiang-He Feng,*[d] and Jian Zhou ✪ *[ace]

Materials with spin dimers have attracted much attention in the last several decades because they could provide a playground to embody simple quantum spin models. For example, the Bose–Einstein condensation of magnons has been observed in $TlCuCl_3$ with anti-ferromagnetic Cu_2Cl_6 dimers. In this work, we have synthesized a new kind of single-crystal $Li_{11}RbGd_4Te_6O_{30}$ with Gd_2O_{15} dimers. This material belongs to the rhombohedral system with the lattice parameters: $a = b = c = 16.0948$ Å and $\alpha = \beta = \gamma = 33.74°$. First-principles calculations indicate that $Li_{11}RbGd_4Te_6O_{30}$ is a wide-bandgap (about 4.5 eV) semiconductor. But unlike many other well studied quantum dimer magnets with an anti-ferromagnetic ground state, the Gd_2O_{14} dimers in $Li_{11}RbGd_4Te_6O_{30}$ show ferromagnetic intra-dimer exchange interactions according to our calculations. Our work provides a new material which could possibly extend the studies of the spin dimers.

1. Introduction

Dimerized quantum spin systems are one of the simplest physical models in quantum mechanisms.[1] They are closely related to many phenomena associated with condensed matter physics. For example, the widely concerned quantum dimer magnet (QDM) is a quantum magnetism in which a pair of spins are entangled and form an $S = 0$ singlet state. The singlet ground states act like bosons and their excited triplet states (also called triplons) can undergo Bose–Einstein condensation (BEC), which is one of the most exotic phenomena predicted by quantum mechanics.[2,3] Many quantum dimer magnet systems have been reported in the past several decades. A canonical example of a strongly coupled spin-dimer system is $TlCuCl_3$. It is a monoclinic structure composed of planar dimers of Cu_2Cl_6, which has a strong antiferromagnetic intra-dimer interaction and a much weaker inter-dimer interaction.[3–5] $BaCuSi_2O_6$ is

a quasi-2D square lattice magnetic insulator with a gapped spin dimer ground state and is supposed to be an ideal candidate for studying the BEC of triplons as a function of the external magnetic field.[6] Recently, Hester *et al.*[7] reported a new Yb^{3+} based QDM in the distorted honeycomb-lattice material $Yb_2Si_2O_7$ with strong spin–orbit coupling (SOC). The intra-dimer bond length of two Yb ions is about 3% shorter than that of the inter-dimer ones, resulting in contrastive exchange interactions $J_{intra} = 0.236$ meV and $J_{inter} = 0.06$ meV.

In addition to BEC, quantum spin dimers are intently associated with other physical phenomena, such as the topologic states research. $SrCu_2(BO_3)_2$ is the archetypal quantum magnet with a gapped dimer-singlet ground state and triplon excitations to realize the Shastry–Sutherland model.[8] The anisotropies arising from the intra-dimer Dzyaloshinskii–Moriya interactions give rise to topological character in the triplon band structure.[9,10] Dimers strongly influence the whole magnetic state of crystal. Generally, an isolated dimer is anti-ferromagnetic coupling and spin dimer materials usually exhibit a quite intricate magnetic property. Jia *et al.*[11] proposed that the breaking bonds in Ge–Ge dimers of $SrCo_2(Ge_{1-x}P_x)_2$ lead to a paramagnetic–ferromagnetic transition. A weakly coupled spin transition metal Cu dimers and Fe chains compound $Cu_2Fe_2Ge_4O_{13}$ exhibits that the Cu dimers play the role of media in the indirect magnetic interaction.[12] Actually, spin dimers mostly consist of transition metal elements. Compared to 3d electrons in transition metal ion systems, the shielding effect of magnetic 4f electrons with Yb dimers in rare earth metal $Cs_3Yb_2Cl_9$ and $Cs_3Yb_2Br_9$ result in smaller exchange interactions, but lead to considerable magnetic dipole–dipole interactions.[13] Spin dimer system is under great focus while

[a]*National Laboratory of Solid State Microstructures, Department of Materials Science and Engineering, Nanjing University, Nanjing, 210093 China. E-mail: zhoujian@nju.edu.cn*

[b]*National Laboratory of Solid State Microstructures, Department of Physics, Nanjing University, Nanjing, 210093 China*

[c]*Collaborative Innovation Center of Advanced Microstructure, Nanjing University, Nanjing, 210093 China*

[d]*State Key Laboratory of Structural Chemistry, Fujian Institute of Research on the Structure of Matter, Chinese Academy of Sciences, Fuzhou 350002, China. E-mail: fengjianghe@fjirsm.ac.cn*

[e]*Jiangsu Key Laboratory of Artificial Functional Materials, Nanjing University, Nanjing, 210093 China*

† Electronic supplementary information (ESI) available. CCDC 1984029 contains the supplementary crystallographic data of $Li_{11}RbGd_4Te_6O_{30}$ for this paper. For ESI and crystallographic data in CIF or other electronic format see DOI: 10.1039/c9ra10163b

dimers of rare earth (RE) metal ions have received much less attention.

Here we report a newly synthesized rare earth metal compound $Li_{11}RbGd_4Te_6O_{30}$ consisting of Gd_2O_{15} dimers. Our first-principles calculations indicate that $Li_{11}RbGd_4Te_6O_{30}$ is a wide-bandgap semiconductor and the Gd^{3+} ions in the same dimer have a ferromagnetic exchange interaction.

2. Experimental methods

2.1. Synthesis and crystal growth of $Li_{11}RbGd_4Te_6O_3$

$Li_{11}RbGd_4Te_6O_{30}$ was synthesized by the high-temperature solid-state reactions. The reagents of Li_2CO_3, Rb_2CO_3, Gd_2O_3, and TeO_2 at the stoichiometric ratio of $11:1:4:12$ were ground in agate mortar before loaded into a platinum crucible. Then the mixture was heated to 820 °C in 10 h, retained for 2 days, and then cooled to 600 °C at 3–5 °C h^{-1} rate, thereafter, cooled to room temperature at rate of 20 °C h^{-1} before the furnace power was switched off. Then colorless and small single crystals can be obtained after the sample being soaked in deionized water for 1 day. Te^{4+} usually can be oxidized to Te^{6+} by oxygen during the reaction at high temperature in air.[14] Furthermore, the EDS elemental analysis on several single crystals shows an average Rb/Te/Gd molar ratio of 1.0/5.8/3.9 (Fig. S1 in the ESI†), which is consistent with that from single-crystal XRD studies. And ICP measurement confirmed the existence of Li-ion in this compound.

2.2. Elemental analyses

Energy-dispersive spectroscopy (EDS) and SEM analyses were accomplished with a JEOL JSM-6700F scanning electron microscope and Hitachi FE-SEM SU8010. Inductively coupled plasma (ICP) measurement was investigated on an Ultima 2 inductively coupled plasma OES spectrometer.

2.3. Single crystal structure determination

Platy single crystal was glued onto glass fiber and mounted on a SuperNova (Mo) X-ray Source ($\lambda = 0.71073$ Å) at 293(2) K for reflection data collections. The data set was corrected for Lorentz, polarization factors and absorption by the Multi-scan method by the CrysAlisPro software,[15] and the R(int) improved from 0.126 (before correction) to be 0.063 (after correction). This structure was solved by direct methods and refined by a full-matrix least-squares fitting on F^2 by using SHELX-2018.[16] All atoms were refined with anisotropic thermal parameters. The structures were checked for possible twinning and missing symmetry elements by using PLATON, but none was found.[17]

2.4. Computational details

Electron properties of $Li_{11}RbGd_4Te_6O_{30}$ are calculated by the density functional theory (DFT) implemented in the Vienna *ab initio* simulation package (VASP).[18,19] The projected augmented wave method[20,21] and the generalized gradient approximation with the Perdew–Burke–Ernzerhof revised for solids (PBEsol) exchange–correlation functional are used.[22] The plane-wave cutoff energy is 520 eV and the Gaussian smearing width is

0.05 eV. Both the internal atomic positions and the lattice constants are allowed to relax until the maximal residual Hellmann–Feynman forces on atoms are smaller than 0.02 eV Å^{-1}. The k-mesh is $2 \times 2 \times 2$ for structural optimization and $4 \times 4 \times 4$ is used for the electron density of states (DOS) calculations. The GGA+U method with the approach described by Dudarev *et al.*[23] is used in our calculations. The effective U of 6.0 eV is used on Gd's f orbitals. Due to the well-known underestimation of bandgap in standard DFT calculations, we also use the modified Becke–Johnson (MBJ) exchange potential,[24] which could yield band gaps with an accuracy similar to hybrid functional or GW methods, but in a much less computational cost. The crystal structures are plotted by the VESTA program.[25]

3. Results and discussion

3.1. Crystal structure

Our synthesized $Li_{11}RbGd_4Te_6O_{30}$ is a colorless and transparent crystal with several hundred-micrometer size (Fig. S2 in the ESI†). It belongs to the rhombohedral system with a space group $R\bar{3}c$ (No. 167). In experiment, it is more convenient to show the structure in a hexagonal representation, as given in Fig. 1a. The experimental refined structural and crystallographic data are summarized in Table 1. The hexagonal cell parameters are $a = b = 9.3415(2)$ Å and $c = 45.4929(15)$ Å. Equivalently, its primitive cell parameters are $a = b = c = 16.0948$ Å and $\alpha = \beta = \gamma = 33.74°$ in the rhombohedral representation. $Li_{11}RbGd_4Te_6O_{30}$ has a very complex crystal structure. Its hexagonal unit cell contains 312 ions and three primitive cells.

The experimental refined atomic coordinates, Wyckoff positions, equivalent isotropic displacement parameters, and important bond lengths are listed in Tables 2 and 3, respectively. It is found that three types of Li ions occupy the 36f, 12c and 18e sites, while Rb ions occupy the 6b site.
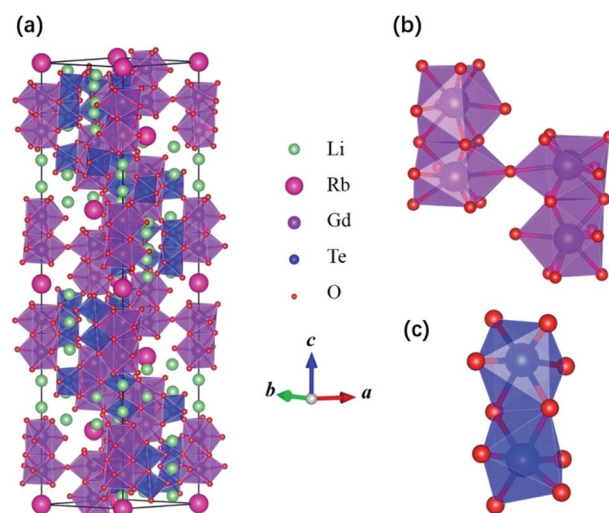

Fig. 1 (a) Hexagonal unit cell of $Li_{11}RbGd_4Te_6O_{30}$ and the local structure of (b) four GdO_9 tetrakaidecahedrons and (c) two TeO_6 octahedrons.

Table 1 Crystallographic data and tructure refinements for $Li_{11}RbGd_4Te_6O_{30}{}^a$

Formula	$Li_{11}RbGd_4Te_6O_{30}$
fw	2036.41
Temp, K	293(2)
Space group	$R\bar{3}c$
a/Å	9.3340(2)
c/Å	45.4665(14)
Volume/Å³	3430.50(15)
Z	6
D_{calc}, g cm⁻³	5.914
$F(000)$	5268
Completeness (%)	99.7
μ, mm⁻¹	21.191
GOF on F^2	1.20
R_1, wR_2 [$I > 2\sigma(I)$]	0.019, 0.0452
R_1, wR_2 (all data)	0.020, 0.0456

^{a} $R_1 = \sum ||F_o| - |F_c||/\sum|F_o|$, w$R_2 = \{\sum w[(F_o)^2 - (F_c)^2]^2/\sum w[(F_o)^2]^2\}^{1/2}$.

Table 2 Atomic coordinates ($\times10^{-4}$), Wyckoff positions, and equivalent isotropic displacement parameters ($\times10^{-3}$ Å²) for $Li_{11}RbGd_4Te_6O_{30}$

Atom	Wyckoff	x	y	z	U (eq.)
Gd(1)	12c	10 000	10 000	771(1)	5(1)
Gd(2)	12c	10 000	10 000	1538(1)	5(1)
Te(1)	36f	6515(1)	10 058(1)	483(1)	4(1)
Rb(1)	6b	10 000	100 000	0	12(1)
Li(1)	12c	6667	13 333	548(4)	10(3)
Li(2)	36f	9875(9)	13 260(9)	213(2)	14(2)
Li(3)	18e	6667	6519(12)	833	17(2)
O(1)	36f	8863(4)	11 287(4)	481(1)	8(1)
O(2)	18e	6667	11 476(4)	833	8(1)
O(3)	18e	6667	8755(5)	833	7(1)
O(4)	36f	6079(4)	11 432(4)	248(1)	9(1)
O(5)	36f	4176(4)	8737(4)	538(1)	7(1)
O(6)	36f	6377(4)	8623(3)	182(1)	8(1)

There are two types of Gd ions both occupying 12c sites and every Gd ions have nine neighboring O ions and forms GdO₉ tetrakaidecahedrons. For Gd(1), the nine Gd–O bonds have three different lengths: 2.340, 2.361 and 2.738 Å, while the bond

Table 4 Theoretical optimized lattice constants and volume of hexagonal cell of $Li_{11}RbGd_4Te_6O_{30}$

Lattice constant	a (Å)	c (Å)	V (Å³)
Theory	9.3098	45.4157	3408.93

lengths of Gd(2)–O are shorter, which are 2.326, 2.505, and 2.512 Å. Two Gd–O tetrakaidecahedrons (Gd(1) and Gd(2)) along the c axis share the same face and forms a Gd₂O₁₅ dimer structure. In the a–b plane, two Gd–O tetrakaidecahedrons are also connected by the same O ion. The local structure of four GdO₉ tetrakaidecahedrons is separately shown in Fig. 1b. The intra-dimer distance between the two Gd ions in the same dimer is about 3.5 Å, which is much shorter than that of the inter-dimer Gd ions (about 5.4 Å).

The Te ions occupy the 36f site and every Te ion is surrounded by six O ions and forms TeO₆ octahedron. The Te–O bond lengths spread from 1.864 to 2.051 Å. The two TeO₆ octahedrons along the c axis share the same edge and form a Te₂O₁₀ dimer structure, which is shown in Fig. 1c.

Based on the experimental crystal structure, we also implemented a theoretical structural optimization based on the DFT calculation. Both the lattice constants and atomic positions are optimized in a primitive cell. We find the theoretical lattice constants are well consistent with the experimental ones with a maximal error of 0.34% as shown in Table 4. The theoretical atomic positions are also in good agreement with the experimental results, which are not shown here.

3.2. Electronic structure

In order to understand the basic physical properties of Li_{11}-$RbGd_4Te_6O_{30}$, we also calculated its band structure and electronic density of states (DOS) by the first-principles calculations. In general, the normal DFT method cannot deal with the lanthanides correctly due to their strongly correlation of the f electrons. However, in the crystal $Li_{11}RbGd_4Te_6O_{30}$, the Gd ions have a valence state of 3⁺. A Gd³⁺ ion has 7 electrons, which just fully occupy the majority f orbitals and make the minority f orbitals totally empty (*i.e.* Gd³⁺ has a high spin state and a spin

Table 3 Selected bond lengths (Å), bond valence (BV) and bond valence sum (BVS) for $Li_{11}RbGd_4Te_6O_{30}$

Bond	Distances	BV	BVS	Bond	Distances	BV	BVS
Gd(1)–O(5)×3	2.340(3)	0.476	3.261	Rb(1)–O(1)×6	2.938(3)	0.160	0.816
Gd(1)–O(1) × 3	2.361(3)	0.449		Rb(1)–O(6) × 6	3.070(3)	0.112	
Gd(1)–O(3) × 3	2.738(2)	0.162		Li(1)–O(4) × 3	2.082(10)	0.189	1.021
Gd(2)–O(4) × 3	2.326(3)	0.476	3.291	Li(1)–O(2) × 3	2.165(9)	0.151	
Gd(2)–O(6) × 3	2.505(3)	0.449		Li(2)–O(1)	2.008(9)	0.231	0.855
Gd(2)–O(5) × 3	2.512(3)	0.162		Li(2)–O(6)	2.069(8)	0.196	
Te(1)–O(4)	1.864(3)	1.1541	5.775	Li(2)–O(6)	2.093(9)	0.184	
Te(1)–O(6)	1.875(3)	1.120		Li(2)–O(4)	2.183(7)	0.1441	
Te(1)–O(1)	1.899(2)	1.050		Li(2)–O(5)	2.318(9)	0.100	
Te(1)–O(5)	1.912(2)	1.014		Li(3)–O(3)	2.087(12)	0.187	0.676
Te(1)–O(2)	2.028(2)	0.741		Li(3)–O(5) × 2	2.193(4)	0.140	
Te(1)–O(3)	2.051(2)	0.696		Li(3)–O(1) × 2	2.302(3)	0.105	

magnetic moment of 7 μ_B). As a result, the f bands of Gd ions should be far away from the Fermi energy and thus Gd^{3+} ions could be handled reasonably well in the simple GGA+U scheme.
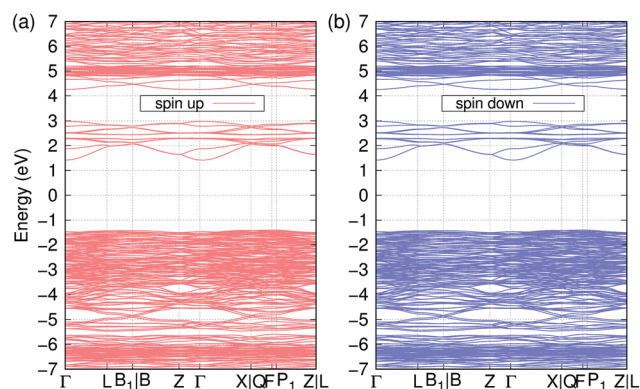
On the other hand, since there are 8 Gd ions in the primitive cell (24 ones in a conventional cell) of the $Li_{11}RbGd_4Te_6O_{30}$ and it is almost not possible to calculate all the magnetic structures in the first-principles calculations. As we show above, the Gd ions in $Li_{11}RbGd_4Te_6O_{30}$ forms dimer structures, it is reasonable to assume that the Gd(1) and Gd(2) in a Gd_2O_{15} dimer has the strongest exchange interaction, while the interactions between different dimmers are weaker. Therefore, we consider eight magnetic configurations in a primitive cell shown in Table 5. The positions of eight Gd ions in the primitive cell are shown in Fig. S3 in the ESI.† The first four configurations in Table 5 have a ferromagnetic intra-dimer coupling while the last four have an anti-ferromagnetic coupling. However, their inter-dimer couplings contain both ferromagnetic and anti-ferromagnetic ones due to the complex connecting relationship between different Gd_2O_{15} dimers. We cannot construct a magnetic configuration with all the inter-dimer coupling being anti-ferromagnetic or ferromagnetic except for the ferromagnetic one (first configuration in Table 5).

The total energies of eight spin configurations are also given in Table 5, from which we can find that the first four configurations have lower energies than those of the last four. Therefore, we could expect that the intra-dimer coupling should be ferromagnetic. However, we cannot determine the size of the inter-dimer coupling due to the complex connecting relationship between different dimers. In our calculations, the spin configuration ↑↑↑↑↓↓↓↓ has the lowest energy, which is 1.1 meV per primitive cell (or 0.28 meV per a Gd_2O_{15} dimer) lower than the ferromagnetic one. Such a small energy difference is reasonable since the f orbitals are quite localized. Furthermore, the calculated spin magnetic moment of Gd ions are 7 μ_B as we expected.

In Fig. 2, we represent the electron band structure of $Li_{11}RbGd_4Te_6O_{30}$ with the ↑↑↑↑↓↓↓↓ spin configuration. It is found that the valence bands are quite flat, while the conduction bands are much dispersive. We also can see that there are lots of flat bands around −6.5 and 5 eV, which is supposed to be the occupied and unoccupied f orbitals of Gd ions respectively. We can confirm it later in the DOS calculations. It is obvious that there is a quite large bandgap of 2.8 eV in both spin components.

Table 5 Eight calculated spin configurations in a primitive cell from Gd1 to Gd8. The positions of eight Gd ions are shown in Fig. S3. The ↑ and ↓ symbols represent spin up and down respectively. The total energy (per primitive cell) of the ferromagnetic configuration is 0

No.	Spin structure	Relative energy (meV)
1	↑↑↑↑↑↑↑↑	0
2	↑↑↑↑↑↑↓↓	−0.96
3	↑↑↑↑↓↓↓↓	−1.10
4	↑↑↓↓↓↓↓↓	−0.83
5	↑↓↑↓↑↓↑↓	1.23
6	↑↓↑↓↑↓↓↑	1.03
7	↑↓↑↓↓↑↓↑	0.03
8	↑↓↓↑↑↑↓↑	0.82

Fig. 2 Spin-polarized band structure of $Li_{11}RbGd_4Te_6O_{30}$ with the ↑↑↑↑↓↓↓↓ spin configuration calculated based on the GGA+U method. The Fermi energy, located at the middle of the bandgap, is set to zero.

The normal DFT method always underestimate the band gap significantly in semiconductors or insulators. Therefore we also use the MBJ method to obtain a more accurate bandgap. The MBJ calculation results in a much larger bandgap of about 4.5 eV. Since the crystal of $Li_{11}RbGd_4Te_6O_{30}$ is quite transparent in the visible light, we think that the experimental band gap should be close to 4.5 eV as we obtained in the MBJ calculation.

In Fig. 3, we present the total and partial electron DOS of $Li_{11}RbGd_4Te_6O_{30}$ in the same magnetic state as used in Fig. 2. It is obvious that the electron states near the Fermi energy are both mainly contributed from O's p orbitals (red). There are two narrow peaks (blue) near −6.5 and 5 eV which are of course the Gd's f orbitals. The DOS of other ions such as Rb, Li, and Te are not shown here since their states are far away from the Fermi energy.

3.3. Discussions

The Gd^{3+} ions are in high spin states which is confirmed by the first-principles calculations. The exchange interaction between
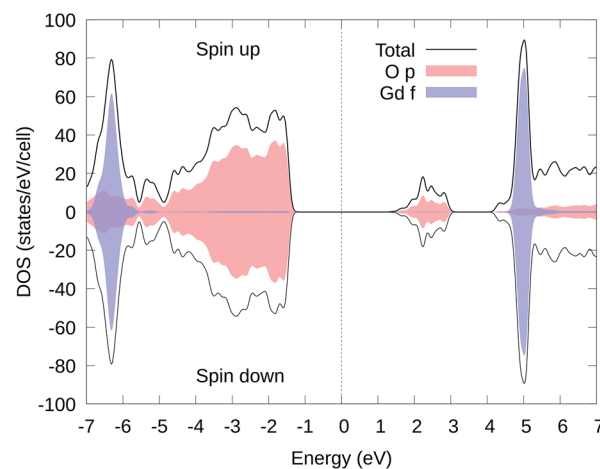
Fig. 3 Spin-polarized electron DOS of $Li_{11}RbGd_4Te_6O_{30}$ with the ↑↑↑↑↓↓↓↓ spin configuration. The total DOS of the primitive cell is represented by the black solid line. The red and blue color represent the DOS of oxygen's p orbitals and Gd's f orbitals respectively. The Fermi energy, located at the middle of the bandgap, is set to zero.

the two Gd ions in the same dimer is shown to be ferromagnetic, however, we still can see that the inter-dimer coupling can not be negligible. From Table 5, it is obvious that the first four spin configurations all have a ferromagnetic coupling in the same dimer but they have different total energies due to the different inter-dimer coupling. This is because the smallest inter-dimer distance (about 5.4 Å) is not that much longer than the intra-dimer one (about 3.5 Å), thus the inter-dimer coupling can not be negligible. However, we can not determine the size of the inter-dimer coupling at present due to the complex crystal structure. From Table 5, we can conclude that the ferromagnetic order is not favored in theory. More experimental works about the magnetic properties of $Li_{11}RbGd_4Te_6O_{30}$ should be taken in the future. Nevertheless, the strength of the magnetic coupling is very small due to the much-localized f orbitals of Gd. If $Li_{11}RbGd_4Te_6O_{30}$ has a long-range magnetic order, its Néel temperature should be quite low.

4. Conclusions

We have synthesized a new rhombohedral crystal $Li_{11}RbGd_4Te_6O_{30}$ with Gd_2O_{15} dimer structures. Our experimental refinements and theoretical optimizations give almost the same lattice constants and atomic positions. This indicates that we have obtained a highly reliable crystal structure for the very complex crystal $Li_{11}RbGd_4Te_6O_{30}$. Its preliminary electronic and magnetic properties are only studied by the first-principles calculations. It is found that $Li_{11}RbGd_4Te_6O_{30}$ is a wide-bandgap (about 4.5 eV) semiconductor. Gd^{3+} ions are in high spin states with a spin magnetic moment of 7 μ_B. The exchange interactions between the two Gd^{3+} ions in the same Gd_2O_{15} dimer are ferromagnetic from our calculations. The inter-dimer couplings can not be negligible but are not determined in the present work. More experimental works about the magnetic properties of Li_{11}-$RbGd_4Te_6O_{30}$ should be taken in the future. This material could possibly extend the studies of the spin dimers.

Conflicts of interest

The authors declare no competing financial interest.

Acknowledgements

References

1 D. S. Inosov, *Adv. Phys.*, 2018, **67**, 149–252.

2 T. Giamarchi, C. Rüegg and O. Tchernyshyov, *Nat. Phys.*, 2008, **4**, 198–204.

3 F. Yamada, T. Ono, H. Tanaka, G. Misguich, M. Oshikawa and T. Sakakibara, *J. Phys. Soc. Jpn.*, 2008, **77**, 4–7.

4 T. Nikuni, M. Oshikawa, A. Oosawa and H. Tanaka, *Phys. Rev. Lett.*, 2000, **84**, 5868.

5 A. Oosawa, T. Kato, H. Tanaka, K. Kakurai, M. Müller and H. J. Mikeska, *Phys. Rev. B*, 2002, **65**, 094426.

6 M. Jaime, V. F. Correa, N. Harrison, C. D. Batista, N. Kawashima, Y. Kazuma, G. A. Jorge, R. Stern, I. Heinmaa, S. A. Zvyagin, Y. Sasago and K. Uchinokura, *Phys. Rev. Lett.*, 2004, **93**, 087203.

7 G. Hester, H. S. Nair, T. Reeder, D. R. Yahne, T. N. DeLazzer, L. Berges, D. Ziat, J. R. Neilson, A. A. Aczel, G. Sala, J. A. Quilliam and K. A. Ross, *Phys. Rev. Lett.*, 2019, **123**, 027201.

8 B. S. Shastry and B. Sutherland, *Phys. B+C*, 1981, **108**, 1069–1070.

9 O. Cépas, K. Kakurai, L. P. Regnault, T. Ziman, J. P. Boucher, N. Aso, M. Nishi, H. Kageyama and Y. Ueda, *Phys. Rev. Lett.*, 2001, **87**, 167205.

10 J. Romhányi, K. Penc and R. Ganesh, *Nat. Commun.*, 2015, **6**, 6805.

11 S. Jia, P. Jiramongkolchai, M. R. Suchomel, B. H. Toby, J. G. Checkelsky, N. P. Ong and R. J. Cava, *Nat. Phys.*, 2011, **7**, 207–210.

12 T. Masuda, A. Zheludev, B. Sales, S. Imai, K. Uchinokura and S. Park, *Phys. Rev. B*, 2005, **72**, 094434.

13 H. U. Güdel, A. Furrer and H. Blank, *Inorg. Chem.*, 1990, **29**, 4081–4084.

14 J. H. Feng, C. L. Hu, X. Xu, F. Kong and J. G. Mao, *Inorg. Chem.*, 2015, **54**, 2447–2454.

15 CrystalClear, *Version 1.3.5*, Rigaku Corp., The Woodlands, TX, 1999.

16 G. M. Sheldrick, *Acta Crystallogr., Sect. A: Found. Adv.*, 2015, **71**, 3–8.

17 L. A. Spek, *J. Appl. Crystallogr.*, 2003, **36**, 7–13.

18 G. Kresse and J. Furthmüller, *Comput. Mater. Sci.*, 1996, **6**, 15–50.

19 G. Kresse and J. Furthmüller, *Phys. Rev. B: Condens. Matter Mater. Phys.*, 1996, **54**, 11169.

20 P. E. Blöchl, *Phys. Rev. B: Condens. Matter Mater. Phys.*, 1994, **50**, 17953.

21 D. Joubert, *Phys. Rev. B: Condens. Matter Mater. Phys.*, 1999, **59**, 1758.

22 J. P. Perdew, A. Ruzsinszky, G. I. Csonka, O. A. Vydrov, G. E. Scuseria, L. A. Constantin, X. Zhou and K. Burke, *Phys. Rev. Lett.*, 2008, **100**, 136406.

23 S. Dudarev, G. Botton, S. Y. Savrasov, C. J. Humphreys and A. P. Sutton, *Phys. Rev. B: Condens. Matter Mater. Phys.*, 1998, **57**, 1505.

24 A. D. Becke and E. R. Johnson, *J. Chem. Phys.*, 2006, **124**, 221101.

25 K. Momma and F. Izumi, *J. Appl. Crystallogr.*, 2011, **44**, 1272–1276.